Cell Reports

Article

iPSC Modeling of RBM20-Deficient DCM Identifies Upregulation of RBM20 as a Therapeutic Strategy

Graphical Abstract

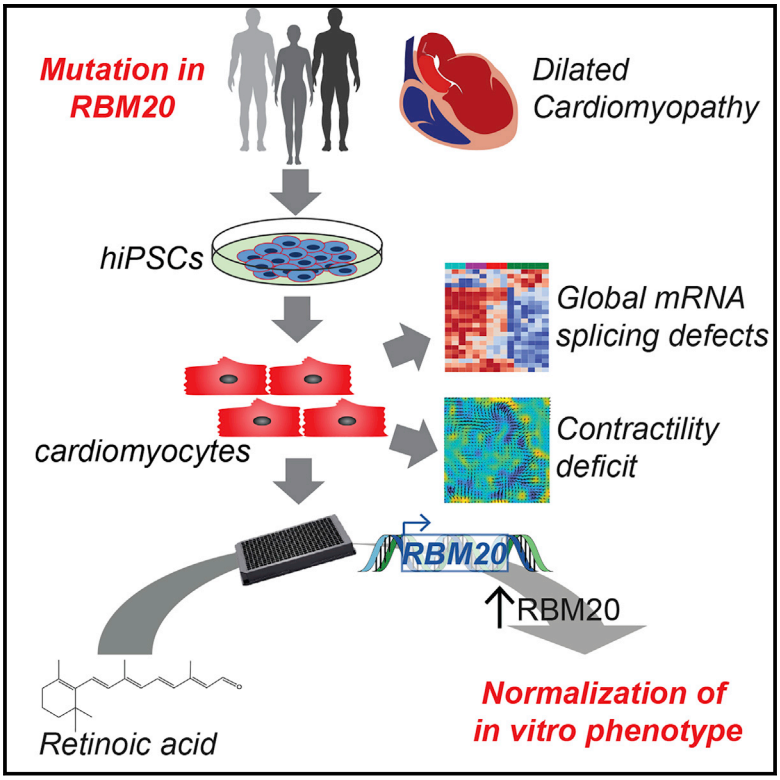

Highlights

- RBM20 mutant DCM iPSC-cardiomyocytes show mRNA splicing and contractile defects
- RBM20 P633L variant causes the phenotypes of the disease
- All-*trans* retinoic acid upregulates RBM20 mRNA and protein expression
- Pharmacological RBM20 upregulation ameliorates DCM phenotypes *in vitro*

Authors

Francesca Briganti, Han Sun, Wu Wei, ..., Michael Gotthardt, Mark Mercola, Lars M. Steinmetz

Correspondence

mmercola@stanford.edu (M.M.), larsms@stanford.edu (L.M.S.)

In Brief

Briganti et al. use iPSC and CRISPR/Cas9 to create a model of RBM20-deficient dilated cardiomyopathy (DCM) that recapitulates mRNA splicing and contractile defects of the disease. They evaluate pharmacological upregulation of *RBM20* as a therapeutic strategy. All-*trans* retinoic acid upregulates RBM20 expression and ameliorates the *in vitro* hallmarks of disease.

Briganti et al., 2020, Cell Reports *32*, 108117
September 8, 2020 © 2020 The Authors.
https://doi.org/10.1016/j.celrep.2020.108117

CellPress

Cell Reports

CellPress
OPEN ACCESS

Article

iPSC Modeling of RBM20-Deficient DCM Identifies Upregulation of RBM20 as a Therapeutic Strategy

Francesca Briganti,[1,2,3,4,15] Han Sun,[3,15] Wu Wei,[5] Jingyan Wu,[3] Chenchen Zhu,[3] Martin Liss,[6] Ioannis Karakikes,[7] Shannon Rego,[3] Andrea Cipriano,[8] Michael Snyder,[3] Benjamin Meder,[5,9] Zhenyu Xu,[10] Gilles Millat,[11] Michael Gotthardt,[6,12,13] Mark Mercola,[4,*] and Lars M. Steinmetz[1,3,4,5,14,16,*]

[1]European Molecular Biology Laboratory (EMBL), Genome Biology Unit, Heidelberg, Germany
[2]Collaboration for joint PhD degree between EMBL and Heidelberg University, Faculty of Biosciences, Heidelberg, Germany
[3]Department of Genetics, School of Medicine, Stanford University, Stanford, CA, USA
[4]Cardiovascular Institute and Department of Medicine, Stanford University, Stanford, CA, USA
[5]Stanford Genome Technology Center, Stanford University, Palo Alto, CA, USA
[6]Neuromuscular and Cardiovascular Cell Biology, Max Delbrück Center for Molecular Medicine, Berlin, Germany
[7]Cardiovascular Institute and Department of Cardiothoracic Surgery, Stanford University, Stanford, CA, USA
[8]Department of Obstetrics and Gynecology, Stanford University, Stanford, CA, USA
[9]Institute for Cardiomyopathies Heidelberg and Department of Internal Medicine III, University of Heidelberg, Heidelberg, Germany
[10]SOPHiA Genetics, St. Sulpice, Switzerland
[11]Laboratoire de Cardiogénétique Moléculaire, Centre de Biologie et Pathologie Est, Hospices Civils de Lyon, Lyon, France
[12]Department of Cardiology, Charité-Universitätsmedizin Berlin, Berlin, Germany
[13]DZHK: German Center for Cardiovascular Research, Partner Site Berlin, Berlin, Germany
[14]DZHK: German Center for Cardiovascular Research, Partner Site EMBL Heidelberg, Heidelberg, Germany
[15]These authors contributed equally
[16]Lead Contact
*Correspondence: mmercola@stanford.edu (M.M.), larsms@stanford.edu (L.M.S.)
https://doi.org/10.1016/j.celrep.2020.108117

SUMMARY

Recent advances in induced pluripotent stem cell (iPSC) technology and directed differentiation of iPSCs into cardiomyocytes (iPSC-CMs) make it possible to model genetic heart disease *in vitro*. We apply CRISPR/Cas9 genome editing technology to introduce three *RBM20* mutations in iPSCs and differentiate them into iPSC-CMs to establish an *in vitro* model of RBM20 mutant *dilated cardiomyopathy* (DCM). In iPSC-CMs harboring a known causal *RBM20* variant, the splicing of RBM20 target genes, calcium handling, and contractility are impaired consistent with the disease manifestation in patients. A variant (Pro633Leu) identified by exome sequencing of patient genomes displays the same disease phenotypes, thus establishing this variant as disease causing. We find that all-*trans* retinoic acid upregulates *RBM20* expression and reverts the splicing, calcium handling, and contractility defects in iPSC-CMs with different causal *RBM20* mutations. These results suggest that pharmacological upregulation of RBM20 expression is a promising therapeutic strategy for DCM patients with a heterozygous mutation in *RBM20*.

INTRODUCTION

Dilated cardiomyopathy (DCM) is characterized by enlargement of the left ventricle and reduced systolic function (Hershberger et al., 2010). Its incidence is estimated at 1 in 250 individuals, making DCM a leading cause of heart failure (Yancy et al., 2013) and the most common indication for heart transplantation (Japp et al., 2016). Heart transplantation is indicated for patients with end-stage DCM, but access is limited, and the procedure is not appropriate for all patients. Despite an improvement in patient outcomes after transplantation over the past 20 years, development of comorbidities remains a serious problem and the 10-year survival rate is just above 50% (Lund et al., 2017).

Thirty to fifty percent of DCM cases involve inherited mutations located in more than 50 individual genes, including many that affect sarcomeric proteins and contractile function (Kinnamon et al., 2017; McNally and Mestroni, 2017; Wilcox and Hershberger, 2018). These genes are thought to partially explain the variable clinical presentation, age of disease onset, and outcome (Hershberger et al., 2013). Patient genetics does not yet play a major role in guiding treatment decisions for inherited DCM (Hershberger et al., 2013). Emerging evidence, however, supports the use of genetics to identify individuals at increased risk for disease progression, congestive heart failure, and arrhythmia as well as for selecting therapeutic strategies (Hershberger et al., 2013). Induced pluripotent stem cells (iPSCs)

This is an open access article under the CC BY-NC-ND license (http://creativecommons.org/licenses/by-nc-nd/4.0/).

derived from patients or harboring mutations introduced by CRISPR genome editing offer a means to develop or select personalized therapeutics. There exist numerous examples of disease-relevant phenotypes that have been reproduced *in vitro* using cardiomyocytes differentiated from iPSCs (iPSC-CMs) derived from patients (Wyles et al., 2016). Here, we have used patient iPSC-CMs as a genetic tool to provide proof-of-concept for a mechanism-based therapeutic strategy.

Mutations in the splicing factor RBM20 cause a severe form of inherited DCM associated with early onset, end-stage heart failure (also in younger patients) and increased incidence of sudden death (Hey et al., 2019; Parikh et al., 2019; Streckfuss-Bömeke et al., 2017). Disease severity is consistent with the physiological function of *RBM20* in regulating heart-specific splicing of many genes essential for the function of cardiac muscle, many of which are also linked to cardiac disease such as *TTN*, *CAMK2D*, and *RYR2* (Beraldi et al., 2014; Guo et al., 2012; Maatz et al., 2014; Streckfuss-Bömeke et al., 2017; Wyles et al., 2016).

We studied a previously uncharacterized variant in RBM20 (Pro633Leu; P633L) that co-segregated with DCM and compared it to another variant classified as disease-causing. We used iPSC-CMs to establish that the P633L variant causes errors in mRNA splicing and pathological contractility associated with RBM20-deficient DCM. We identified all-*trans* retinoic acid (ATRA) as a potential regulator of RBM20. We showed that ATRA increases *RBM20* expression and with high-throughput physiological recording demonstrated that it ameliorates the cellular defects, suggesting that transcriptional upregulation might be therapeutically beneficial for patients with RBM20-deficient DCM.

RESULTS

Linkage Analysis Identifies DCM-Causing Mutation in *RBM20*

We identified a family with familial DCM (Figure 1A), where the grandfather (I;3), father (II;4), and uncle (II;7) of the proband (III;4) passed away with diagnoses of DCM at ages 74, 69, and 53, respectively. In addition, an aunt (II;6) was diagnosed with DCM. The proband presented with a mildly dilated left ventricle and a mildly reduced ejection fraction in 2002. The mother was unaffected by DCM. To identify the disease-causing mutation in this family, we performed exome sequencing on the proband, his father (II;4), his mother (II;3), and his aunt (II;6) (Figure S1A). We found 21,170 variants that were present in father, aunt, and son but not in the mother. We did not find any previously reported DCM-causing mutations. We then examined variants in genes previously linked to DCM (Janin et al., 2018) (Figure S1B). There were five variants in three genes occurring at a frequency of less than 5% in the 1000 Genomes Project and having a missense effect on protein sequences: *TTN*, *LDB3*, and *RBM20* (Table S1). The variants in *TTN* and *LDB3* had been reported and annotated as benign, likely benign, or as variants of unknown significance. Independently, we performed panel sequencing on the father (II;4) in which we targeted 95 prevalent sudden cardiac death-related genes (Chanavat et al., 2016). Both strategies identified a missense mutation in *RBM20* adjacent to a known mutation hotspot in the highly evolutionarily conserved RS domain (arginine/serine-rich domain) (Figures 1B and 1C) (Brauch et al., 2009; Li et al., 2010). The mutation is a proline-to-leucine change at amino acid position 633 (P633L) (Figure S1C). All of the immediately following positions in RBM20, from amino acid 634 to 638, have been previously associated with familial DCM (Brauch et al., 2009; Guo et al., 2012; Li et al., 2010).

To evaluate the pathogenic potential of the P633L mutation independently of the genomic background of the patient, we applied CRISPR/Cas9 to generate a set of isogenic iPSC lines (Figure 1D). In an iPSC line derived from a healthy individual, we introduced either the P633L mutation, the Arg634Gln (R634Q) mutation, previously described as pathogenic (Brauch et al., 2009), or a frameshift mutation at position 635 (Ser635FrameShift [S635FS]) that results in the formation of a premature stop codon and consequent loss of function consistent with a knockout (KO) (Figures S1D–S1J) (Miller and Pearce, 2014). Each edit resulted in homozygous mutations. One clone that underwent the genome editing procedure without gaining a mutation in the *RBM20* gene was selected and utilized as an additional healthy control (named wild-type [WT]; in addition to the unedited parental line, WT-NC). All the iPSC lines were differentiated into iPSC-CMs via modulation of WNT signaling as previously described (Burridge et al., 2014), selected via glucose starvation, and then matured for 4 more weeks before each experiment (Figure 1E) (Feyen et al., 2020).

RBM20 Mutant iPSC-CMs Exhibit Aberrant Splicing

To evaluate the impact of the P633L mutation on RBM20-dependent splicing, we performed RNA sequencing (RNA-seq) analysis on the iPSC-CMs from each genotype (Figure S2A). Alternative splicing events were inferred from the RNA-seq data using DEXSeq with significant hits being further filtered on percent spliced-in (PSI) calculations. All the RBM20-WT lines clustered together, independent of whether they went through the genome editing process (Figure 2A). All the mutant lines clustered together. The PSI plot of *CAMK2D* in Figure S2B shows different exon preference between WT and RBM20 mutant iPSC-CMs. Aberrant splicing of *TTN* and *RyR2* was confirmed by real-time PCR (Figures S2C–S2F). These mis-splicing events correspond to the mis-spliced exons previously described for DCM mutations (Beraldi et al., 2014; Guo et al., 2012; Maatz et al., 2014; Streckfuss-Bömeke et al., 2017; Wyles et al., 2016). To test for P633L-specific splicing defects, we directly compared this line to the R634Q and the S635FS lines. We did not find any significant differences in the target gene sets between the mutants despite the P633L mutation having a less severe effect on splicing (Figure 2A). To evaluate the splicing patterns of patient cells, we generated iPSC-CMs from the proband (DCM1) and compared the splicing of selected RBM20 targets to the splicing patterns of WT and S635FS iPSC-CMs. Figure 2B shows an intermediate splicing phenotype of the heterozygous mutant DCM1 iPSC-CMs lying between the WT and the homozygous S635FS for *TTN* and *CAMK2D*.

RBM20 Mutant iPSC-CMs Show Impaired Calcium and Contractile Function

DCM patients exhibit a significant reduction in left ventricle fractional shortening during systole (Hershberger et al., 2010). To

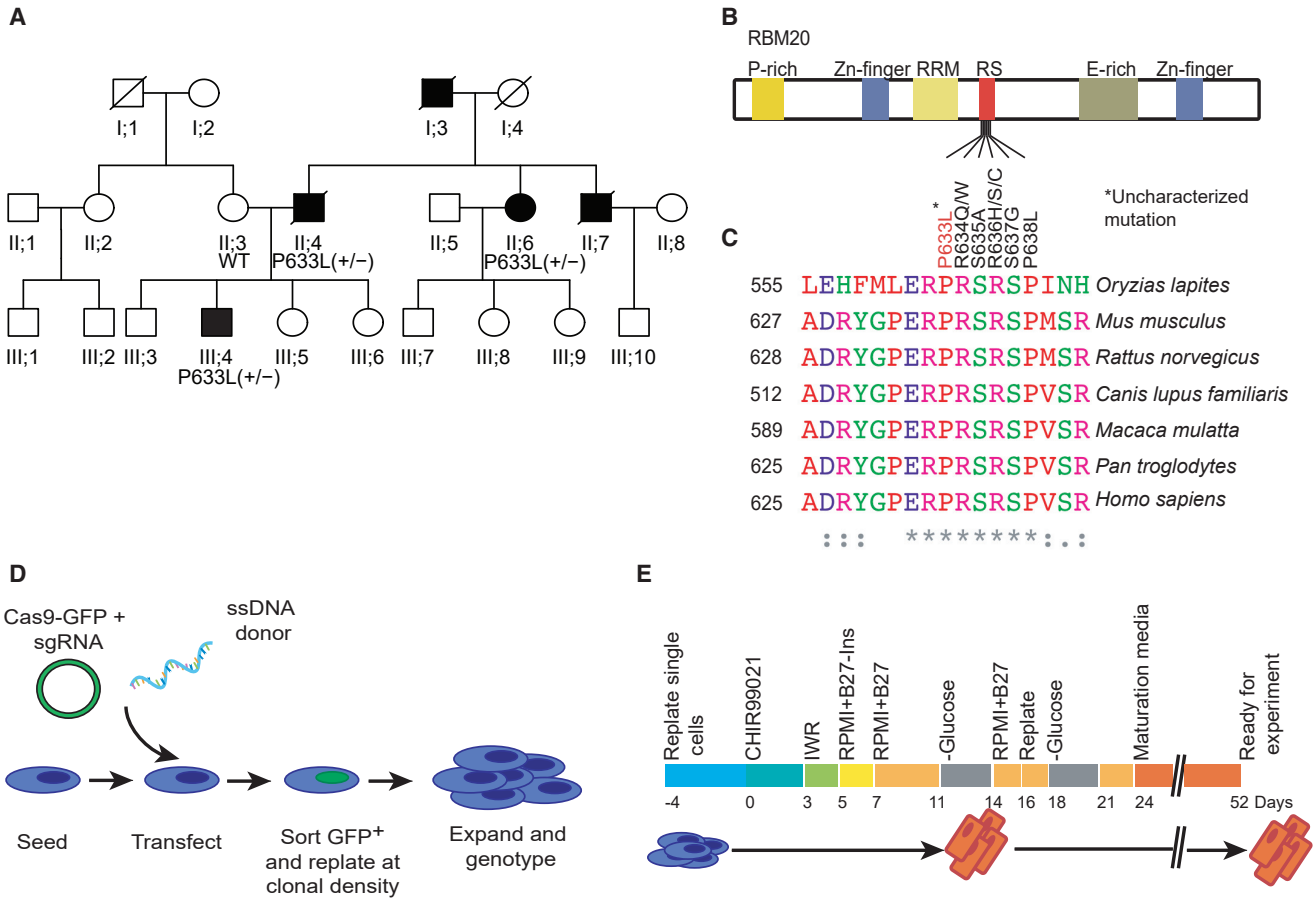

Figure 1. Identification of a Previously Uncharacterized Mutation in the RS Region of *RBM20* in a Family with Inherited DCM

(A) Family pedigree of the proband. Square, male; circle, female; black, affected; white, unaffected; slash through the symbol, deceased; (+), mutant allele; (−), wild-type allele.

(B) Schematic representation of RBM20 protein with predicted functional domains: P-rich, proline rich; Zn finger, Zinc finger domain; RRM, RNA-recognition motif; RS, arginine/serine-rich domain; E-rich, glutamate rich. The previously reported mutations in the RS domain are indicated. The mutation identified by this study is shown in red text and marked with an asterisk (*).

(C) Alignment of *RBM20* from human and six other vertebrates. Residues conserved between human *RBM20* and these species are indicated by an asterisk (*).

(D) Schematic of genome editing strategy. ssDNA, single-stranded DNA; sgRNA, single guide RNA.

(E) Schematic of cardiomyocytes differentiation from iPSCs, annotated with the corresponding media supplementations. CHIR99021 is RPMI + B27-Ins + CHIR99021; IWR is RPMI + B27-Ins + IWR; −Glucose is RPMI −Glucose + B27.

evaluate whether the P633L mutation causes a clinically relevant phenotype in our system, iPSC-CMs were assayed for contractility (representative recordings for WT and the P633L mutant can be seen in Video S1). Contractile function was reduced in all mutant lines, as measured by maximum displacement at systole (Figure 2C). To evaluate the contractile function of patient cells, we examined iPSC-CMs from the proband (DCM1) and his father (DCM2). In both lines, contractile function was significantly reduced (Figure 2C).

It has been proposed that a reduced calcium release from the sarcoplasmic reticulum impairs heart contraction (Marks, 2003). Many of the RBM20 targets are involved in calcium handling. To test whether calcium handling was altered in *RBM20* mutants, we assayed iPSC-CMs for calcium transients (representative recordings for WT and the P633L mutant can be seen in Video S1). Calcium upstroke was significantly slower in the mutated lines with a stronger effect in homozygous than heterozygous lines (Figure 2D).

Retinoic Acid Upregulates RBM20 Expression and Corrects Splicing Defects

We hypothesized that transcriptional upregulation of *RBM20* could be a therapeutic strategy to compensate for loss of function of a heterozygous mutated allele. We interrogated the Gene Expression Atlas database (Petryszak et al., 2014) for conditions that upregulate *RBM20* and found that ATRA treatment was associated with upregulation of *RBM20* expression in human embryonic stem cells in a genome-wide dataset (Colleoni et al., 2011). We confirmed that ATRA can induce upregulation of RBM20 transcript and protein in murine myoblast C2C12 cells (Figures 3A–3C). ATRA treatment of C2C12 cells induced skipping of RBM20-regulated *TTN* exons, although the effect was not

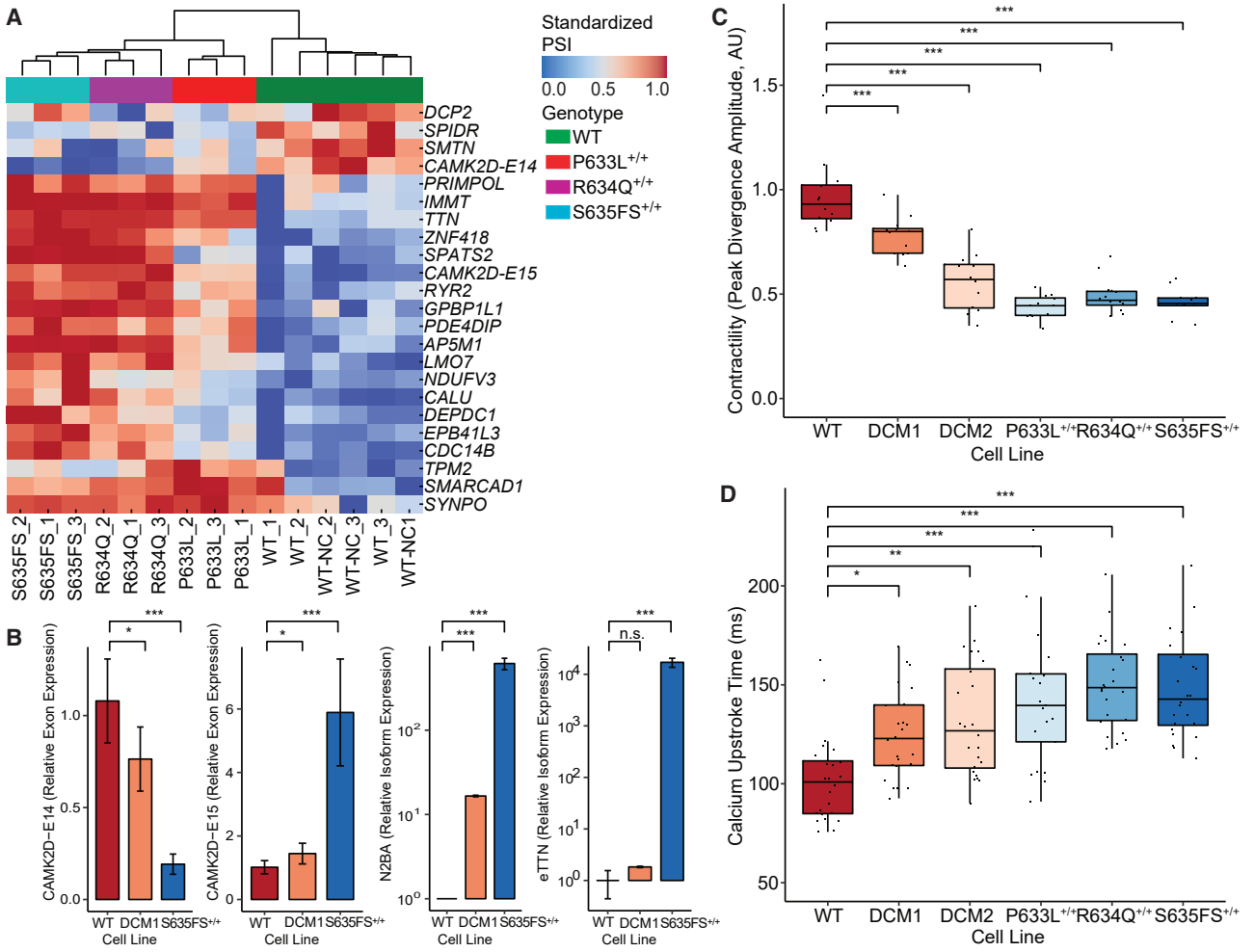

Figure 2. *In Vitro* Model of RBM20-Deficient DCM Recapitulates Molecular and Cellular Defects Relevant to Pathogenesis

(A) Heatmap of PSI values for genes affected by *RBM20* mutations. For *TTN*, the most affected exon is displayed. WT is the unedited iPSC line; WT-NC is the parental line.

(B) qPCR results for selected RBM20-targets (*CAMK2D* and *TTN*) in WT, DCM1, and S635FS iPSC-CM (n = 6). Data are presented as mean ± SD.

(C) Time-series-based analysis of contractile profiles of *RBM20* WT and mutant iPSC-CMs (n = 12). AU, arbitrary unit.

(D) Time-series-based analysis of calcium transients. Upstroke time is the calcium influx time in WT and RBM20 mutant iPSC-CMs (n = 18). (n.s., non-significant; padj, adjusted p value; *padj < 0.05, **padj < 0.01, ***padj < 0.001). (+), mutant allele; (−), wild-type allele.

significant (Figure 3D). We thus evaluated ATRA in a more sensitive RBM20-dependent *TTN* splicing reporter assay in HEK293 cells (Liss et al., 2018) and observed an increase in RBM20 activity as determined by a decrease of the firefly luciferase (FLuc) signal normalized to Renilla luciferase (RLuc) (Figure S3A). ATRA treatment caused a dose-dependent reduction of the FLuc signal in the absence of exogenous RBM20 (Figure S3A). In the presence of exogenous RBM20, firefly luciferase was decreased only at ATRA concentrations exceeding 0.15 μM (Figure S4A). To evaluate RBM20-independent effects of ATRA on the luciferase-based splicing reporter, we tested its effect on the RBM20 independent titin exon Mex4-6 reporter (Maatz et al., 2014). No effect was observed on this second reporter (Figure S3B). These data suggest that ATRA exerts its effects on splicing through RBM20.

To test the effect of ATRA on human iPSC-CMs, we treated WT and patient-derived iPSC-CMs with ATRA. Upon ATRA treatment, we observed dose-dependent upregulation of the *RBM20* transcript in all the lines (Figures 4A, S3C, and S3D). In addition, other known ATRA targets such as *GATA4*, *CYP26B1*, *RARA*, *RARB*, *WNT5A*, and *BRINP2* were upregulated on the transcript level as determined by RNA-seq (Figures S3E and S3F; Table S2). To confirm that upregulation of *RBM20* transcript levels in iPSC-CMs was sufficient to induce upregulation of RBM20 protein, we generated a knockin mCherry tag of endogenous RBM20 in iPSCs. We differentiated these cells into iPSC-CMs and treated them with two different doses of ATRA. Upon 72 h ATRA treatment, we observed a significant increase in mCherry fluorescence (Figures S4A and S4B). To evaluate whether the upregulation of *RBM20* was sufficient to revert the splicing defects, we analyzed *TTN* and *CAMK2D* splicing and observed a moderate but consistent correction of aberrant splicing in *TTN* and *CAMK2D* upon ATRA treatment (Figures 4B, S4C, and

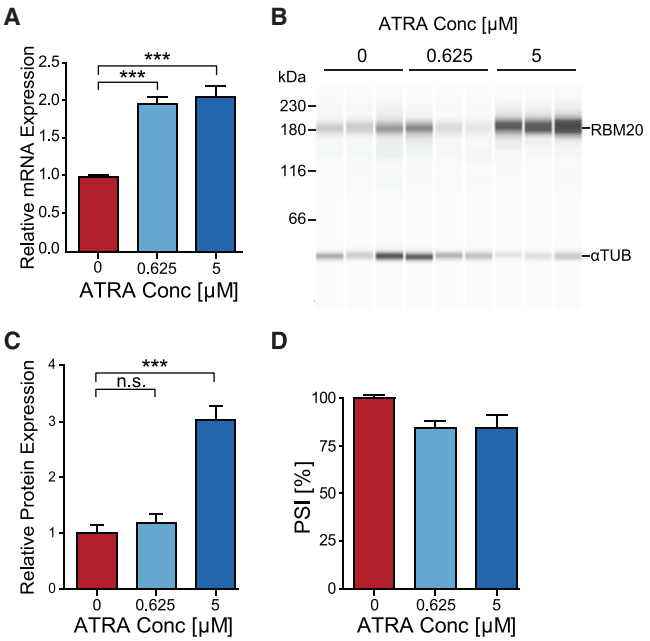

Figure 3. ATRA Upregulates *RBM20* Expression

(A) qRT-PCR analysis of *RBM20* expression in C2C12 upon treatment with different doses of ATRA. Tubulin alpha is used as endogenous control (n = 3). Data are presented as mean ± SD.

(B) Western blot analysis of RBM20 protein after treatment of C2C12 cells with 0.625 and 5 μM ATRA. Tubulin alpha is used as loading control.

(C) Densitometric analysis of RBM20 signal normalized to tubulin alpha signal for the western blot in (B). Data are presented as mean ± SD.

(D) PSI of titin IG exons 241 to 243 in C2C12 at different concentrations of ATRA. PSI, percent spliced-in (n = 3). Data are presented as mean ± SD.

S4D; Table S3). Therefore, *RBM20* expression and activation of RBM20-dependent splicing were induced by ATRA in all cellular systems we tested.

Pharmacological Upregulation of *RBM20* Leads to Amelioration of Contractile and Calcium Handling Defects

To determine whether ATRA-mediated correction of the splicing defects improved the DCM phenotype, we measured calcium handling and contractile function in human iPSC-CMs. Upon ATRA treatment, we observed a dose-dependent reduction of calcium upstroke time in iPSC-CMs DCM1 and DCM2 (Figures 4C and S4F). The homozygous engineered isogenic lines, P633L and R634Q, produced a similar effect (Figures 4C and S4F). No response was observed in the homozygous line S635FS (Figures 4C and S4F). The S635FS mutation produces a premature stop codon, resulting in presumably a functional KO. Consistent with this interpretation, ATRA treatment in these cells did not produce any beneficial effect on *TTN* and *CAMK2D* splicing despite increasing *RBM20* mRNA expression (Figure S4E). Therefore, the lack of rescue by ATRA in the homozygous line S635FS suggests that the improved phenotype in the other mutant lines was dependent on residual RBM20 activity. Upon ATRA treatment of DCM1 and DCM2 iPSC-CMs, in parallel with the reduction in calcium upstroke time, we observed a significant increase in contractility (Figures 4D and S4G). A slight increase in contractility was observed in the homozygous engineered isogenic lines, P633L and R634Q (although not significant for these samples). Because no improvement was observed in the KO iPSC-CMs, improvement in contractility upon ATRA treatment appeared to be RBM20-dependent. Although high doses of ATRA have been shown to be toxic to some cells (Colleoni et al., 2011), our results suggest that cardiomyocytes tolerate this treatment regimen well because they showed no signs of cell death, and the contractile function of the *RBM20* mutant cardiomyocytes improved relative to untreated controls.

DISCUSSION

We identified P633L as a pathogenic variant in RBM20 and evaluated its effect on cardiac-specific splicing. P633L mutant iPSC-CMs showed aberrant splicing of previously described RBM20 targets, including *TTN*, *CAMK2D*, and *RYR2* (Beraldi et al., 2014; Guo et al., 2012; Maatz et al., 2014; Streckfuss-Bömeke et al., 2017; Wyles et al., 2016), as well as defects in contractility and calcium handling. At the molecular level, RBM20 mutations have been reported to impair interactions with other spliceosomal proteins (Maatz et al., 2014). Three lines of evidence have suggested that RBM20 mutations act through a haploinsufficiency mechanism. First, heart failure patients with high expression of *RBM20* have more correctly spliced targets whereas those with low *RBM20* levels have an increased incidence of splicing defects similar to those observed in patients with *RBM20* mutations (Maatz et al., 2014). Second, the amount of splicing of the *TTN* reporter in HEK293 cells has been shown to be RBM20 dose-dependent (Guo et al., 2012). Third, in a genetic rat model, homozygous *RBM20* mutant rats have a more severe phenotype than heterozygous rats (Maatz et al., 2014). Because all patients with RBM20 mutations described to date are heterozygous (the other allele being functional), we reasoned that transcriptional upregulation of *RBM20* would be beneficial. Similar approaches of gene expression upregulation in haploinsufficiency have been beneficial in disease models of Dravet syndrome (Hsiao et al., 2016) and vascular stenosis (Zhang et al., 2012).

ATRA is an active metabolite of vitamin A. It acts as a morphogen in early development during which it plays an essential role in the formation of the anteroposterior and dorsoventral axes. During development, levels of ATRA that are too low or too high are detrimental (Colleoni et al., 2011). After birth, vitamin A is important for a number of physiological functions including vision and immunity (Sommer, 2008). By analyzing the transcriptomics data from embryonic stem cells treated with ATRA (Colleoni et al., 2011), we identified RBM20 as one of the genes upregulated upon ATRA treatment. We found that ATRA upregulated RBM20 in iPSC-CMs and partially reverted the splicing and contractile defect of the affected mutant iPSC-CMs (Figure 4). This proof-of-concept suggests that the upregulation of RBM20 may be a viable therapeutic strategy for RBM20-DCM. With respect to ATRA, the doses used here (5–10 μM) are in range of the plasma concentrations for cancer chemotherapy that have well-known side effects (Castaigne et al., 1993). Nonetheless, RBM20-DCM is progressive with no specific treatment

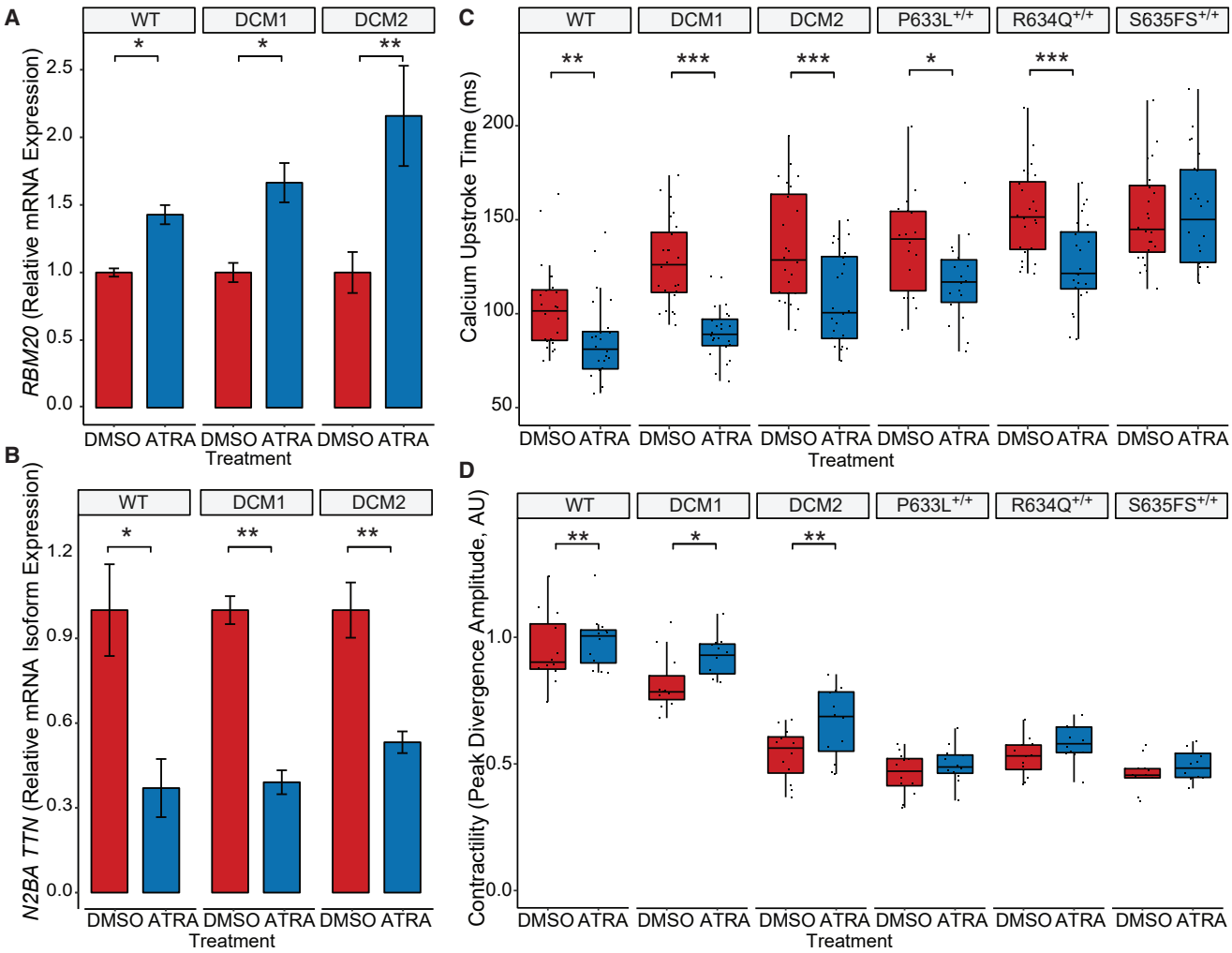

Figure 4. ATRA Reverts the DCM Phenotypes in iPSC-CM

(A) Relative gene expression measured via qRT-PCR for *RBM20* upon DMSO or 10 μM ATRA treatment in WT- and patient-derived iPSC-CMs (n = 6–8). TATA-box binding protein (TBP) is used as endogenous control and gene expression is plotted relative to their respective DMSO controls. Data are presented as mean ± SD.

(B) N2BA *TTN* isoform expression upon DMSO or 10 μM ATRA treatment in WT- and patient-derived iPSC-CMs (n = 6–8). N2BA expression is normalized to total *TTN* expression. The WT DMSO sample is set to 1. Data are presented as mean ± SD.

(C) Time-series-based analysis of calcium transients of RBM20 WT and mutant iPSC-CMs upon 10 μM ATRA treatment. Upstroke time is the calcium influx time (n = 18–24).

(D) Time-series-based analysis of contractile profiles of RBM20 WT and mutant iPSC-CMs upon 10 μM ATRA treatment (n = 12). AU, arbitrary unit; padj, adjusted p value (*padj < 0.05, **padj < 0.01, ***padj < 0.001); (+), mutant allele; (−), wild-type allele.

options, and for this reason, our results suggest that consideration should be given to clinically evaluate ATRA doses ranging from levels recommended as a dietary supplement to potentially toxic levels with appropriate monitoring for side effects.

ATRA did not improve calcium handling or contractility in the homozygous S635FS mutant that lacks splicing activity (Figures 4C, 4D, and S4E–S4G). Therefore, we conclude that the beneficial effect of ATRA was dependent on the presence of residual RBM20 activity. We also found that ATRA partially ameliorated the calcium handling defect of the homozygous mutant iPSC-CMs (P633L and R634Q). We did not detect a significant improvement of the contractility defect in the homozygous point mutation lines, although a trend in this direction was visible. It is possible that the point mutants retain some residual function and their upregulation contributes to the therapeutic effect of ATRA, but this is insufficient to significantly ameliorate the contractility defect in these homozygous mutant iPSC-CMs. To our knowledge, only heterozygous pathogenic mutations in *RBM20* have been identified so far (Parikh et al., 2019). It is possible that homozygous and compound heterozygous pathogenic mutations in *RBM20* result in a more severe phenotype that would be incompatible with postnatal life.

The precise mechanism by which ATRA upregulated *RBM20* is uncertain. There is no consensus retinoic acid responsive element in the promoter region of *RBM20*, suggesting that an indirect effect might be responsible for upregulating *RBM20*

expression. Previously published chromatin immunoprecipitation sequencing (ChIP-seq) data revealed three cardiac-specific transcription factors (GATA4, TB5, and NKX2-5) that bind to the promoter region of *RBM20* in murine cardiomyocytes (Luna-Zurita et al., 2016). Regulation by these factors is consistent with the *RBM20* expression pattern in development (Beraldi et al., 2014) and at the tissue level (Maatz et al., 2014). Indeed, *GATA4* is induced by ATRA as shown by others (Arceci et al., 1993) and our own data (Figure S3E). By analyzing published microarray data (GSE52317 from van Berlo et al. [2013]), we found that *RBM20* expression was reduced upon cardiac-specific *GATA4* depletion in adult mouse hearts *in vivo*. Further studies are necessary to investigate the effect of *GATA4* loss-of-function on RBM20-dependent splicing.

The use of genome editing technologies in combination with *in vitro* differentiation of human iPSCs to evaluate pathogenicity of variants identified in patients is emerging as a promising diagnostic tool. Its value has been shown recently in studies of variants related to channelopathy (Garg et al., 2018) and laminopathy (Lee et al., 2019). Our data use this technology to assess the pathogenicity of a DCM-causing missense mutation in *RBM20*.

In our system, several genes' splicing is affected by mutations in *RBM20*. These findings agree with and extend previous work. Determining the splicing targets of RBM20 is non-trivial. A conserved set of 31 genes were inferred from RNA-seq data on both human and rat cells (Guo et al., 2012) while 18 direct RBM20-bound genes were identified by HITS-CLIP on rat cardiomyocytes (Maatz et al., 2014), with only four genes, including *TTN*, *CAMK2D*, *LDB3*, and *SORBS1*, overlapping both datasets. Among these four genes, we observe mis-splicing of *TTN* and *CAMK2D* and observe mis-splicing of the same exons previously reported (Maatz et al., 2014; van den Hoogenhof et al., 2018).

Calcium mishandling in *RBM20* mutant cardiomyocytes has been attributed to the function of RBM20 as a splicing-regulator of several calcium handling genes including *CAMK2D* and *CACNA1C* (Maatz et al., 2014; Streckfuss-Bömeke et al., 2017; van den Hoogenhof et al., 2018; Wyles et al., 2016). We (Figures 2A and S2D), and others (Streckfuss-Bömeke et al., 2017; Wyles et al., 2016), found that RBM20 regulated the splicing of a small exon (24 bp) in *RyR2*, which plays a major role in the release of calcium from the sarcoplasmic reticulum (SR) and triggers cardiac contraction. This exon was shown to regulate subcellular localization of the protein (George et al., 2007). Despite aberrant splicing of calcium handling proteins, the physiological consequences of RBM20 mutation on iPSC-CM contractility has not been detected. We confirmed aberrant splicing of *RYR2* (Figure S2D) and were able to detect reduced contractility (Figure 2C) and delayed calcium upstroke (Figure 2D). We attribute our ability to detect the pathophysiological consequences to (1) isogenic controls that match the mutant cell and hence increase sensitivity and specificity of the effects, and (2) the increased reliance on sarcoplasmic reticulum Ca^{2+} in our iPSC-CMs that were cultured in the presence of oxidative substrates, which increases sarcoplasmic reticulum Ca^{2+} load relative to iPSC-CMs maintained under glycolytic conditions (Feyen et al., 2020) (STAR Methods). Aberrant regulation of *CAMK2D*, *RYR2*, and cytosolic calcium play a central role in susceptibility to ventricular arrhythmia (Bers, 2014). Given that ATRA had a normalizing effect on *CAMK2D* as well as on calcium dynamics, it is tempting to speculate that it might also normalize the arrhythmogenic propensity of RBM20 mutant DCM.

In summary, the CRISPR-engineered iPSC-CMs model of RBM20-deficient DCM revealed molecular and cellular phenotypes relevant to DCM pathogenesis, including defective contractility and calcium transients. We found that ATRA increased *RBM20* gene expression. Moreover, treatment with ATRA partially reverted the *in vitro* DCM phenotypes. Our data support upregulation of endogenous RBM20 as a therapeutic strategy for RBM20-deficient-DCM.

Limitations of Study

RBM20 mutations result in an arrhythmogenic form of DCM. We have not evaluated the P633L variant iPSC-CMs for proarrhythmic potential, but noted both the R634Q and P633L iPSC-CMs have splicing alterations that are predicted to result in altered CAMK2D and RYR2 proteins (Figure 2A). These proteins mediate a positive feedback circuit involved in ventricular arrhythmia (Bers, 2014), and *CAMK2D* splicing is reverted by ATRA (Figures S4C and S4D). It will be interesting to explore if P633L RBM20 mutant iPSC-CMs display proarrhythmic calcium features as noted previously for the R634Q variant (Wyles et al., 2016) and whether these are reverted by ATRA. In addition, our data indicate that the mechanism of ATRA is transcriptional upregulation of *RBM20* leading to an increase in the protein expression (Figures 3, 4A, S3C, and S3D) that compensates for a functional deficit. How this upregulation occurs, and whether additional mechanisms can be targeted to boost RBM20 expression or activity, is the focus of ongoing studies.

STAR★METHODS

Detailed methods are provided in the online version of this paper and include the following:

- KEY RESOURCES TABLE
- RESOURCE AVAILABILITY
  - Lead Contact
  - Material Availability
  - Data and Code Availability
- EXPERIMENTAL MODELS AND SUBJECT DETAILS
  - Human samples
  - Cardiomyocyte differentiation and treatment
  - HEK cells maintenance and transfection
  - C2C12 maintenance
- METHOD DETAILS
  - Linkage analysis in a family with familial DCM
  - Genome editing
  - Splicing Reporter Assay
  - Protein analysis
  - RNA sequencing
  - qRT-PCR
  - Image acquisition
  - Image analysis and calculation of physiological parameters
- QUANTIFICATION AND STATISTICAL ANALYSIS

SUPPLEMENTAL INFORMATION

Supplemental Information can be found online at https://doi.org/10.1016/j.celrep.2020.108117.

ACKNOWLEDGMENTS

The authors would like to thank Dr. Guangwen Wang, director of Stanford University Stem Cell Core, for assistance in reprogramming patient cells. This work was supported by the Steinmetz Cardiomyopathy Fund (to L.M.S., in memory of Michael Steinmetz), by the Joan and Sanford I. Weill Scholar Endowment (to M.M.), by the NIH (HG000205 to L.M.S. and R01HL138539, R01HL130840, R01HL13967901, R21HL141019, and P01HL141084 to M.M.), the NIH National Center for Advancing Translational Science Clinical and Translational Science Award (UL1TR001085 to L.M.S.), the NIH Common Fund Human Microbiome Project (HMP) (1U54DE02378901 to M.S.), BMBF (CaRNAtion to M.G.), DFG (to M.G.), and the Berry Foundation Fellowship (to J.W.). The content is solely the responsibility of the authors and does not necessarily represent the official views of the NIH.

AUTHOR CONTRIBUTIONS

F.B. designed and performed the CRISPR, PCR, and cellular phenotyping experiments. F.B. and H.S. analyzed the results. H.S., W.W., and C.Z. analyzed and interpreted the exome sequencing results and reviewed all the statistical analyses. H.S. performed the linkage analysis. S.R. and M.S. coordinated clinical sample collection. J.W. prepared the RNA sequencing libraries. Z.X. and G.M. performed independent targeted clinical sequence validation of the DCM2 sample. I.K. designed the CRISPR editing experiments. M.L. and M.G. designed and performed *in vitro* analysis of ATRA on HEK and C2C12 cells. A.C. carried out the promoter analysis. B.M. advised on cell phenotyping results. F.B., M.M., and L.M.S. designed the experiments, interpreted the data, and wrote the manuscript. All authors commented on the manuscript. L.M.S. conceived the study and supervised the inter-institutional collaboration.

DECLARATION OF INTERESTS

L.M.S. is co-founder and shareholder of Sophia Genetics. F.B., H.S., W.W., and L.M.S. have submitted a patent application on "Methods of treatment, genetic screening, and disease models for heart conditions associated with *RBM20* deficiency." M.M. is a shareholder of Vala Science.

Received: April 11, 2020
Revised: July 11, 2020
Accepted: August 17, 2020
Published: September 8, 2020

REFERENCES

Anders, S., Reyes, A., and Huber, W. (2012). Detecting differential usage of exons from RNA-seq data. Genome Res. *22*, 2008–2017.

Andrews, S. (2010). FastQC: a quality control tool for high throughput sequence data (Babraham Bioinformatics).

Arceci, R.J., King, A.A., Simon, M.C., Orkin, S.H., and Wilson, D.B. (1993). Mouse GATA-4: a retinoic acid-inducible GATA-binding transcription factor expressed in endodermally derived tissues and heart. Mol. Cell. Biol. *13*, 2235–2246.

Beraldi, R., Li, X., Martinez Fernandez, A., Reyes, S., Secreto, F., Terzic, A., Olson, T.M., and Nelson, T.J. (2014). Rbm20-deficient cardiogenesis reveals early disruption of RNA processing and sarcomere remodeling establishing a developmental etiology for dilated cardiomyopathy. Hum. Mol. Genet. *23*, 3779–3791.

Bers, D.M. (2014). Cardiac sarcoplasmic reticulum calcium leak: basis and roles in cardiac dysfunction. Annu. Rev. Physiol. *76*, 107–127.

Brauch, K.M., Karst, M.L., Herron, K.J., de Andrade, M., Pellikka, P.A., Rodeheffer, R.J., Michels, V.V., and Olson, T.M. (2009). Mutations in ribonucleic acid binding protein gene cause familial dilated cardiomyopathy. J. Am. Coll. Cardiol. *54*, 930–941.

Burridge, P.W., Matsa, E., Shukla, P., Lin, Z.C., Churko, J.M., Ebert, A.D., Lan, F., Diecke, S., Huber, B., Mordwinkin, N.M., et al. (2014). Chemically defined generation of human cardiomyocytes. Nat. Methods *11*, 855–860.

Burridge, P.W., Holmstrom, A., and Wu, J.C. (2015). Chemically Defined Culture and Cardiomyocyte Differentiation of Human Pluripotent Stem Cells. Curr. Protoc. Hum. Genet. *87*, 21.3.1–21.3.15.

Castaigne, S., Lefebvre, P., Chomienne, C., Suc, E., Rigal-Huguet, F., Gardin, C., Delmer, A., Archimbaud, E., Tilly, H., Janvier, M., et al. (1993). Effectiveness and pharmacokinetics of low-dose all-trans retinoic acid (25 mg/m2) in acute promyelocytic leukemia. Blood *82*, 3560–3563.

Cerignoli, F., Charlot, D., Whittaker, R., Ingermanson, R., Gehalot, P., Savchenko, A., Gallacher, D.J., Towart, R., Price, J.H., McDonough, P.M., and Mercola, M. (2012). High throughput measurement of Ca^{2+} dynamics for drug risk assessment in human stem cell-derived cardiomyocytes by kinetic image cytometry. J. Pharmacol. Toxicol. Methods *66*, 246–256.

Chanavat, V., Janin, A., and Millat, G. (2016). A fast and cost-effective molecular diagnostic tool for genetic diseases involved in sudden cardiac death. Clin. Chim. Acta *453*, 80–85.

Colleoni, S., Galli, C., Gaspar, J.A., Meganathan, K., Jagtap, S., Hescheler, J., Sachinidis, A., and Lazzari, G. (2011). Development of a neural teratogenicity test based on human embryonic stem cells: response to retinoic acid exposure. Toxicol. Sci. *124*, 370–377.

Dobin, A., Davis, C.A., Schlesinger, F., Drenkow, J., Zaleski, C., Jha, S., Batut, P., Chaisson, M., and Gingeras, T.R. (2013). STAR: ultrafast universal RNA-seq aligner. Bioinformatics *29*, 15–21.

Feyen, D.A.M., McKeithan, W.L., Bruyneel, A.A.N., Spiering, S., Hörmann, L., Ulmer, B., Zhang, H., Briganti, F., Schweizer, M., Hegyi, B., et al. (2020). Metabolic Maturation Media Improve Physiological Function of Human iPSC-Derived Cardiomyocytes. Cell Rep. *32*, 107925.

Garg, P., Oikonomopoulos, A., Chen, H., Li, Y., Lam, C.K., Sallam, K., Perez, M., Lux, R.L., Sanguinetti, M.C., and Wu, J.C. (2018). Genome Editing of Induced Pluripotent Stem Cells to Decipher Cardiac Channelopathy Variant. J. Am. Coll. Cardiol. *72*, 62–75.

George, C.H., Rogers, S.A., Bertrand, B.M.A., Tunwell, R.E.A., Thomas, N.L., Steele, D.S., Cox, E.V., Pepper, C., Hazeel, C.J., Claycomb, W.C., and Lai, F.A. (2007). Alternative splicing of ryanodine receptors modulates cardiomyocyte Ca2+ signaling and susceptibility to apoptosis. Circ. Res. *100*, 874–883.

Guo, W., Schafer, S., Greaser, M.L., Radke, M.H., Liss, M., Govindarajan, T., Maatz, H., Schulz, H., Li, S., Parrish, A.M., et al. (2012). RBM20, a gene for hereditary cardiomyopathy, regulates titin splicing. Nat. Med. *18*, 766–773.

Hershberger, R.E., Morales, A., and Siegfried, J.D. (2010). Clinical and genetic issues in dilated cardiomyopathy: a review for genetics professionals. Genet. Med. *12*, 655–667.

Hershberger, R.E., Hedges, D.J., and Morales, A. (2013). Dilated cardiomyopathy: the complexity of a diverse genetic architecture. Nat. Rev. Cardiol. *10*, 531–547.

Hey, T.M., Rasmussen, T.B., Madsen, T., Aagaard, M.M., Harbo, M., Mølgaard, H., Møller, J.E., Eiskjær, H., and Mogensen, J. (2019). Pathogenic RBM20-Variants Are Associated With a Severe Disease Expression in Male Patients With Dilated Cardiomyopathy. Circ. Heart Fail. *12*, e005700.

Hsiao, J., Yuan, T.Y., Tsai, M.S., Lu, C.Y., Lin, Y.C., Lee, M.L., Lin, S.W., Chang, F.C., Liu Pimentel, H., Olive, C., et al. (2016). Upregulation of Haploinsufficient Gene Expression in the Brain by Targeting a Long Non-coding RNA Improves Seizure Phenotype in a Model of Dravet Syndrome. EBioMedicine *9*, 257–277.

Janin, A., Bessière, F., Chauveau, S., Chevalier, P., and Millat, G. (2018). First identification of homozygous truncating CSRP3 variants in two unrelated cases with hypertrophic cardiomyopathy. Gene *676*, 110–116.

Japp, A.G., Gulati, A., Cook, S.A., Cowie, M.R., and Prasad, S.K. (2016). The Diagnosis and Evaluation of Dilated Cardiomyopathy. J. Am. Coll. Cardiol. *67*, 2996–3010.

Kinnamon, D.D., Morales, A., Bowen, D.J., Burke, W., and Hershberger, R.E.; DCM Consortium* (2017). Toward Genetics-Driven Early Intervention in Dilated Cardiomyopathy: Design and Implementation of the DCM Precision Medicine Study. Circ. Cardiovasc. Genet. *10*, e001826.

Lee, J., Termglinchan, V., Diecke, S., Itzhaki, I., Lam, C.K., Garg, P., Lau, E., Greenhaw, M., Seeger, T., Wu, H., et al. (2019). Activation of PDGF pathway links LMNA mutation to dilated cardiomyopathy. Nature *572*, 335–340.

Li, H., and Durbin, R. (2009). Fast and accurate short read alignment with Burrows-Wheeler transform. Bioinformatics *25*, 1754–1760.

Li, H., Handsaker, B., Wysoker, A., Fennell, T., Ruan, J., Homer, N., Marth, G., Abecasis, G., and Durbin, R.; 1000 Genome Project Data Processing Subgroup (2009). The Sequence Alignment/Map format and SAMtools. Bioinformatics *25*, 2078–2079.

Li, D., Morales, A., Gonzalez-Quintana, J., Norton, N., Siegfried, J.D., Hofmeyer, M., and Hershberger, R.E. (2010). Identification of novel mutations in RBM20 in patients with dilated cardiomyopathy. Clin. Transl. Sci. *3*, 90–97.

Liao, Y., Smyth, G.K., and Shi, W. (2014). featureCounts: an efficient general purpose program for assigning sequence reads to genomic features. Bioinformatics *30*, 923–930.

Liss, M., Radke, M.H., Eckhard, J., Neuenschwander, M., Dauksaite, V., von Kries, J.P., and Gotthardt, M. (2018). Drug discovery with an RBM20 dependent titin splice reporter identifies cardenolides as lead structures to improve cardiac filling. PLoS ONE *13*, e0198492.

Livak, K.J., and Schmittgen, T.D. (2001). Analysis of relative gene expression data using real-time quantitative PCR and the 2(-Delta Delta C(T)) Method. Methods *25*, 402–408.

Love, M.I., Huber, W., and Anders, S. (2014). Moderated estimation of fold change and dispersion for RNA-seq data with DESeq2. Genome Biol. *15*, 550.

Luna-Zurita, L., Stirnimann, C.U., Glatt, S., Kaynak, B.L., Thomas, S., Baudin, F., Samee, M.A., He, D., Small, E.M., Mileikovsky, M., et al. (2016). Complex Interdependence Regulates Heterotypic Transcription Factor Distribution and Coordinates Cardiogenesis. Cell *164*, 999–1014.

Lund, L.H., Khush, K.K., Cherikh, W.S., Goldfarb, S., Kucheryavaya, A.Y., Levvey, B.J., Meiser, B., Rossano, J.W., Chambers, D.C., Yusen, R.D., and Stehlik, J.; International Society for Heart and Lung Transplantation (2017). The Registry of the International Society for Heart and Lung Transplantation: Thirty-fourth Adult Heart Transplantation Report-2017; Focus Theme: Allograft ischemic time. J. Heart Lung Transplant. *36*, 1037–1046.

Maatz, H., Jens, M., Liss, M., Schafer, S., Heinig, M., Kirchner, M., Adami, E., Rintisch, C., Dauksaite, V., Radke, M.H., et al. (2014). RNA-binding protein RBM20 represses splicing to orchestrate cardiac pre-mRNA processing. J. Clin. Invest. *124*, 3419–3430.

Marks, A.R. (2003). Calcium and the heart: a question of life and death. J. Clin. Invest. *111*, 597–600.

McKenna, A., Hanna, M., Banks, E., Sivachenko, A., Cibulskis, K., Kernytsky, A., Garimella, K., Altshuler, D., Gabriel, S., Daly, M., and DePristo, M.A. (2010). The Genome Analysis Toolkit: a MapReduce framework for analyzing next-generation DNA sequencing data. Genome Res. *20*, 1297–1303.

McNally, E.M., and Mestroni, L. (2017). Dilated Cardiomyopathy: Genetic Determinants and Mechanisms. Circ. Res. *121*, 731–748.

Miller, J.N., and Pearce, D.A. (2014). Nonsense-mediated decay in genetic disease: friend or foe? Mutat. Res. Rev. Mutat. Res. *762*, 52–64.

Parikh, V.N., Caleshu, C., Reuter, C., Lazzeroni, L.C., Ingles, J., Garcia, J., McCaleb, K., Adesiyun, T., Sedaghat-Hamedani, F., Kumar, S., et al. (2019). Regional Variation in RBM20 Causes a Highly Penetrant Arrhythmogenic Cardiomyopathy. Circ. Heart Fail. *12*, e005371.

Patwardhan, A., Harris, J., Leng, N., Bartha, G., Church, D.M., Luo, S., Haudenschild, C., Pratt, M., Zook, J., Salit, M., et al. (2015). Achieving high-sensitivity for clinical applications using augmented exome sequencing. Genome Med. *7*, 71.

Petryszak, R., Burdett, T., Fiorelli, B., Fonseca, N.A., Gonzalez-Porta, M., Hastings, E., Huber, W., Jupp, S., Keays, M., Kryvych, N., et al. (2014). Expression Atlas update–a database of gene and transcript expression from microarray- and sequencing-based functional genomics experiments. Nucleic Acids Res. *42*, D926–D932.

Picelli, S., Faridani, O.R., Björklund, A.K., Winberg, G., Sagasser, S., and Sandberg, R. (2014). Full-length RNA-seq from single cells using Smart-seq2. Nat. Protoc. *9*, 171–181.

Ran, F.A., Hsu, P.D., Wright, J., Agarwala, V., Scott, D.A., and Zhang, F. (2013). Genome engineering using the CRISPR-Cas9 system. Nat. Protoc. *8*, 2281–2308.

Robinson, J.T., Thorvaldsdóttir, H., Winckler, W., Guttman, M., Lander, E.S., Getz, G., and Mesirov, J.P. (2011). Integrative genomics viewer. Nat. Biotechnol. *29*, 24–26.

Schneider, C.A., Rasband, W.S., and Eliceiri, K.W. (2012). NIH Image to ImageJ: 25 years of image analysis. Nat. Methods *9*, 671–675.

Serrano, R., McKeithan, W.L., Mercola, M., and del Alamo, J.C. (2018). High-Throughput Functional Screening Assay of Force and Stiffness in IPSC Derived Cardiomyocytes. Biophys. J. *114*, 312a.

Sharma, A., Burridge, P.W., McKeithan, W.L., Serrano, R., Shukla, P., Sayed, N., Churko, J.M., Kitani, T., Wu, H., Holmström, A., et al. (2017). High-throughput screening of tyrosine kinase inhibitor cardiotoxicity with human induced pluripotent stem cells. Sci. Transl. Med. *9*, eaaf2584.

Sommer, A. (2008). Vitamin a deficiency and clinical disease: an historical overview. J. Nutr. *138*, 1835–1839.

Streckfuss-Bömeke, K., Tiburcy, M., Fomin, A., Luo, X., Li, W., Fischer, C., Özcelik, C., Perrot, A., Sossalla, S., Haas, J., et al. (2017). Severe DCM phenotype of patient harboring RBM20 mutation S635A can be modeled by patient-specific induced pluripotent stem cell-derived cardiomyocytes. J. Mol. Cell. Cardiol. *113*, 9–21.

van Berlo, J.H., Aronow, B.J., and Molkentin, J.D. (2013). Parsing the roles of the transcription factors GATA-4 and GATA-6 in the adult cardiac hypertrophic response. PLoS ONE *8*, e84591.

van den Hoogenhof, M.M.G., Beqqali, A., Amin, A.S., van der Made, I., Aufiero, S., Khan, M.A.F., Schumacher, C.A., Jansweijer, J.A., van Spaendonck-Zwarts, K.Y., Remme, C.A., et al. (2018). RBM20 Mutations Induce an Arrhythmogenic Dilated Cardiomyopathy Related to Disturbed Calcium Handling. Circulation *138*, 1330–1342.

Wang, K., Li, M., and Hakonarson, H. (2010). ANNOVAR: functional annotation of genetic variants from high-throughput sequencing data. Nucleic Acids Res. *38*, e164.

Wilcox, J.E., and Hershberger, R.E. (2018). Genetic cardiomyopathies. Curr. Opin. Cardiol. *33*, 354–362.

Wyles, S.P., Li, X., Hrstka, S.C., Reyes, S., Oommen, S., Beraldi, R., Edwards, J., Terzic, A., Olson, T.M., and Nelson, T.J. (2016). Modeling structural and functional deficiencies of RBM20 familial dilated cardiomyopathy using human induced pluripotent stem cells. Hum. Mol. Genet. *25*, 254–265.

Yancy, C.W., Jessup, M., Bozkurt, B., Butler, J., Casey, D.E., Jr., Drazner, M.H., Fonarow, G.C., Geraci, S.A., Horwich, T., Januzzi, J.L., et al. (2013). 2013 ACCF/AHA guideline for the management of heart failure: executive summary: a report of the American College of Cardiology Foundation/American Heart Association Task Force on practice guidelines. Circulation *128*, 1810–1852.

Zhang, P., Huang, A., Morales-Ruiz, M., Starcher, B.C., Huang, Y., Sessa, W.C., Niklason, L.E., and Giordano, F.J. (2012). Engineered zinc-finger proteins can compensate genetic haploinsufficiency by transcriptional activation of the wild-type allele: application to Willams-Beuren syndrome and supravalvular aortic stenosis. Hum. Gene Ther. *23*, 1186–1199.

STAR★METHODS

KEY RESOURCES TABLE

REAGENT or RESOURCE	SOURCE	IDENTIFIER
Antibodies		
rabbit polyclonal anti-RBM20	Guo et al., 2012	N/A
anti-αTubulin	Calbiochem	DM1A
Deposited Data		
RNA sequencing dataset	This paper	Sequence Read Archive (SRA): PRJNA579336
Experimental Models: Cell Lines		
Human iPSC line (healthy donor)	SCVI Biobank	SCVI-15S1
Human iPSC- *RBM20 P633L*	This paper	N/A
Human iPSC- *RBM20 R634Q*	This paper	N/A
Human iPSC- *RBM20 S635FS*	This paper	N/A
Human iPSC- *RBM20 WT*	This paper	N/A
Human iPSC- *DCM1*	This paper	N/A
Human iPSC- *DCM2*	This paper	N/A
Human iPSC- *RBM20-mCherry*	Mercola lab	N/A
Oligonucleotides		
Primers used in this study see Table S4	This paper	NA
Recombinant DNA		
pSpCas9(BB)-2A-GFP	Ran et al., 2013	Addgene plasmid # 48138
pUC19	NEB	Cat# C3040H
Luciferase-based splicing	Guo et al., 2012	N/A
Luciferase-based RBM20-independent splicing reporter	Guo et al., 2012	N/A
pcDNA-RBM20	Guo et al., 2012	N/A
Software and Algorithms		
Cytseer software	Vala Sciences	http://www.valasciences.com/
ImageJ	Schneider et al., 2012	https://imagej.nih.gov/ij/
FastQC	Andrews, 2010	https://www.bioinformatics.babraham.ac.uk/projects/fastqc/
Samtools	Li et al., 2009	http://www.htslib.org/
bwa	Li and Durbin, 2009	http://bio-bwa.sourceforge.net/
STAR	Dobin et al., 2013	https://github.com/alexdobin/STAR
featureCounts	Liao et al., 2014	http://subread.sourceforge.net/
GATK	McKenna et al., 2010	https://gatk.broadinstitute.org/hc/en-us
ANNOVAR	Wang et al., 2010	https://doc-openbio.readthedocs.io/projects/annovar/en/latest/
DESeq2	Love et al., 2014	https://bioconductor.org/packages/release/bioc/html/DESeq2.html
DEXSeq	Anders et al., 2012	https://bioconductor.org/packages/release/bioc/html/DEXSeq.html
IGV	Robinson et al., 2011	http://software.broadinstitute.org/software/igv/

RESOURCE AVAILABILITY

Lead Contact

Further information and requests for resources and reagents should be directed to and will be fulfilled by the Lead Contact, Lars Steinmetz (larsms@stanford.edu).

Material Availability

Further information and requests for resources should be directed to and will be fulfilled by the Lead Contact. Unique reagents generated in this study are available from the Lead Contact with a completed Materials Transfer Agreement.

Data and Code Availability

The datasets generated during this study are available at the Sequence Read Archive (SRA) Database with accession number PRJNA579336.

EXPERIMENTAL MODELS AND SUBJECT DETAILS

Human samples

iPSC lines from the proband and his father (DCM1 and DCM2 respectively) were derived at the Stanford Stem Cell Core under the IRB-30064 protocol from blood cells using the Thermo Fisher CytoTune2.0 kit (A16517). Participants gave written informed consent. A control iPSC line was obtained from the Stanford Cardiovascular Institute Biobank.

Cardiomyocyte differentiation and treatment

iPSCs were differentiated into cardiomyocytes as a monolayer and through the modulation of Wnt signaling as previously described (Burridge et al., 2015). Briefly, iPSCs were plated at low density on matrigel coated plates to achieve 70%–80% confluency after 4 days (Day 0 of differentiation) when differentiation was induced with RPMI supplemented with 1XB27 Minus Insulin (Life Technologies 0050129SA) and 6 μM CHIR99021 (TOCRIS 4953). On Day 3, media was replaced with RPMI supplemented with 1XB27 Minus Insulin and 5 μM IWR (Selleckchem S7086). On Day 5, media was replaced with RPMI supplemented with 1XB27 Minus Insulin. From Day 7 to day 11, cells were kept in RPMI supplemented with 1XB27. To increase cardiomyocyte purity, cells were cultured in RPMI without glucose for three days. On day 16, the iPSC-CMs were dissociated with TrypLE 10x and seeded in 6-well Matrigel coated plates at a density of $3x10^6$ per well in RPMI with 1XB27 containing 10% KOSR and ROCK inhibitor Y-27632 (Tocris, Bristol, UK) (replating media). After 2 days, cells were cultured in RPMI with 1XB27 without glucose for 3 days prior to switching to 3ml of a metabolism-based maturation media (Feyen et al., 2020).

All-trans retinoic acid (ATRA) was purchased from Sigma (R 2625) and dissolved in DMSO according to manufacturer's instructions. For gene expression and splicing analysis, cells were treated for 48h with either ATRA or the same volume of DMSO (0.01% v/v). For contractility and calcium assays, cells were treated for 72 hours to allow enough time for the targets to be translated into proteins and accumulate to a significant level. All ATRA handling was performed in the dark and cell culture plates were wrapped in aluminum foil to protect ATRA from light exposure.

HEK cells maintenance and transfection

Human embryonic kidney (HEK293.EBNA) cells (Life Technologies GmbH, Darmstadt, Germany) were maintained in high glucose Dulbecco's modified eagle medium (DMEM) supplemented with 10% fetal bovine serum (Sigma-Aldrich Chemie GmbH, Munich, Germany [F7524, Lot#124M3337]) and 1% penicillin/streptomycin 10,000 U/mL (GIBCO by Life Technologies GmbH, Darmstadt, Germany).

For transfection of HEK cells, 25000 cells/well were seeded on 96-well Nunc F96 MicroWell plates (Life Technologies GmbH, Darmstadt, Germany) and reverse transfected with a total of 60 ng of plasmid DNA per well of which 1 ng was splicing reporter, 1 ng was RBM20 or control plasmid (pcDNA3.1), and 58 ng empty vector pBSSK. To deliver plasmid DNA we used the 160 kDa linear polyethylenimine (Polysciences Europe GmbH, Hirschberg, Germany) at a 1:2.2 ratio (DNA:PEI160). Cells were incubated for 60 h at 37°C in the presence of 5% CO2.

C2C12 maintenance

C2C12 cells (Sigma Aldrich, Munich) were maintained in high glucose Dulbecco's modified eagle medium (DMEM) supplemented with 10% fetal bovine serum (Sigma-Aldrich Chemie GmbH, Munich, Germany [F7524, Lot#124M3337]) and 1% penicillin/streptomycin 10,000 U/mL (GIBCO by Life Technologies GmbH, Darmstadt, Germany).

METHOD DETAILS

Linkage analysis in a family with familial DCM

Exome sequencing for the proband (III;4), his father (II;4), his mother (II;3) and his aunt (II;6) was performed on blood cells. DNA was isolated using Gentra Puregene Kits (QIAGEN) following manufacturer's instructions. Sequencing was performed at Personalis using the ACE Clinical Exome Test, which includes sequencing of selected non-coding regions (Patwardhan et al., 2015). Paired-end sequencing with 2x100 base pair reads was used and an average coverage of 60x was achieved (Figure S1A). The reads were mapped to the human genome reference GRCh37. Single Nucleotide Variants (SNVs) and INDELs were called and filtered using GATK (v3) and further annotated using ANNOVAR (v2015Dec14).

Variants identified as being in common between III;4, II;4, II;6 and absent in II;3, were first filtered by their frequency in the 1000 genome project, with those whose frequency is higher than 5% excluded. Next, the remaining variants were filtered according to their effects on protein sequences, removing those locating in intergenic, intronic, UTR regions, or having synonymous changes. Third, only the variants in the genes related to heart development or heart diseases (101 genes) were retained. Fourth, variants were checked manually in the raw sequence trace files to remove false positive calls. Finally, the remaining variants were checked against the ClinVar database to exclude those annotated as benign, likely benign, or variant of uncertain significance.

Independent clinical sequence validation was carried out on the father (II;4). Genomic DNA was tested by Next-Generation Sequencing (NGS) using a custom design, based on a SeqCap EZ Solution-Based Enrichment strategy (Roche NimbleGen, Madison, Wisconsin). Targeted sequencing capture probes were custom designed by Roche NimbleGen. The panel was designed to identify disease-causing mutations in 48 cardiomyopathy-causing genes (Janin et al., 2018). Target regions included coding exons (padding: 30 bp), as well as 5′- and 3′-UTR regions. Libraries were constructed with the Kapa Library Preparation Kit for Illumina platforms (Kapa Biosystems, London, UK) according to the manufacturer's instructions and further sequenced on a Next-Seq500 sequencer using the NextSeq500 Mid Output Kit v2 (300 cycles) chemistry (Illumina, San Diego, California). *In silico* analysis was performed using a personalized Sophia Genetics pipeline optimized for both single nucleotide polymorphism (SNP)/indels and copy number variation (CNV) detection (Chanavat et al., 2016).

Genome editing

Single guide RNAs were designed using the Feng Zhang lab's CRISPR Design tool (http://zlab.bio/guide-design-resources). Two complementary oligonucleotides making up the gRNA construct were ordered separately (Table S4), annealed in T4 ligation buffer (NEB), and phosphorylated with T4 PNK (NEB). Annealed and phosphorylated oligonucleotides were cloned into the BbsI sites of the pSpCas9(BB)-2A-GFP plasmid and transformed into STBL3 *E. coli* cells. The sequence of the gRNA clones was confirmed by Sanger sequencing.

Human iPSCs were plated into Matrigel coated 6-well plates one day before transfection at low density in Essential 8 (E8) media. On the day of transfection, media was changed to E8 supplemented with Rock inhibitor (Tocris Cat. No. 1254). Cells were transfected with Lipofectamine 3000 following manufacturer's instructions. CRISPR/Cas9 vector (1μ, pSpCas9(BB)-2A-GFP) and 4 μg of single-stranded DNA (ssDNA) donor (Table S4) or 3μg of targeting vector were used for each well of a 6-well plate. GFP+ cells were isolated 36-48 hours after transfection using a FACSAria IIu (DB Biosciences) flow cytometer with a 100-μm nozzle. Cells were plated at a density of 2-3x10^3 cells/well in a 6-well plate in E8 media supplemented with Rock inhibitor. Cells were maintained in E8 media supplemented with Rock inhibitor for the first 3 days and were cultured in regular E8 media until the colonies reached a size of ~0.5 mm. Individual iPSC clones were isolated with the assistance of a stereomicroscope located inside a cell culture cabinet and each clone was re-plated in a well of a 24-well plate in E8 supplemented with Rock inhibitor. A few cells for each clone were resuspended in 20 μL media and used for genomic DNA isolation with 0.5 μL of DNA Release Additive in 20 μL Dilution Buffer (Phire Animal Tissue Direct PCR Kit (Thermo Fisher)). Finally, 2 μL of the mix was used for direct PCR amplification of the target genomic region using PrimeSTAR GXL DNA Polymerase (Clontech).

To confirm that homozygous edits did not result from loss of one of the two alleles, we examined the parental line and found it has three heterozygous variants in the 3′UTR of *RBM20* at positions Chr10:110836524, Chr10:110837082, Chr10:110837531. We analyzed the RNaseq data and found that all three heterozygous variants are present and expressed in all the edited lines.

The top 3 predicted off-targets of the guide RNA were amplified and analyzed via Sanger sequencing to exclude the presence of unwanted editing (data not shown).

For the mCherry-RBM20 knock-in, the mCherry ORF was amplified from pREST-B mCherry using primers mCherry_Fwand mCherryRV (Table S4), and homology recombination arms form human genomic DNA with primers RBM20_RA_FW, RBM20_RA_RV, RBM20_LA_FW, RBM20_LA_RV (Table S4). pUC19 was used as backbone and amplified with primers pUC_FW and pUC_RV (Table S4). The targeting vector was obtained via Gibson assembly.

Splicing Reporter Assay

The reporter assay has previously been described (Guo et al., 2012). We transfect a plasmid expressing wild-type RBM20 (pcDNA3.1RBM20) or empty vector (pcDNA3.1) for reference and compare treatment with compound versus vehicle. Compounds were applied to the microtiter plate in a final volume of 20 μL (1:19) in complete growth medium with 80 μL cell/transfection mix seeded on at the indicated concentrations at a final DMSO concentration of 1%. Luciferase activity was measured 60 hours post-transfection using the Dual-Luciferase® Reporter Assay System (Promega GmbH, Mannheim, Germany) on an Infinite® M200 Pro (TECAN, Maennedorf, Switzerland) plate reader.

Protein analysis

C2C12 cells were harvested using trypsin/EDTA 0.25% for 2 min at 37°C with subsequent downstream processing or snap freezing in liquid nitrogen. For protein extraction, samples were suspended in RIPA buffer (50 mM Tris pH 8.0, 150 mM NaCl, 1% NP-40, 0.25% sodium deoxycholate, 1.0 mM EDTA; 0.1% SDS) and lysed via sonication with 20 bursts at 70% energy using a VialTweeter

(Hielscher Ultrasonics GmbH, Teltow, Germany). Protein concentration was estimated after precipitation of cell debris at 13,000xg for 20 min at 4°C using BCA assay (Life Technologies GmbH, Darmstadt, Germany [23225]). Samples were kept cool at all times.

For quantitation of proteins we used a partially automated Simple Western System (WES), based on capillary electrophoresis with reagents provided by the manufacturer (WES, ProteinSimple, San Jose, CA). They include biotinylated molecular weight marker, streptavidin–HRP fluorescent standards, luminol-S, hydrogen peroxide, sample buffer, DTT, stacking matrix, separation matrix, running buffer, wash buffer, and matrix removal buffer, secondary antibodies, antibody diluent, and capillaries, which we used according to the manufacturer's recommendations. The stock samples were adjusted to working stocks of 2 mg/ml and diluted 10-fold using the 0.1X sample buffer and 5X master mix (200 mM DTT, 5 × sample buffer, 5 × fluorescent standards). Samples were denatured at 95°C for 5 min., and loaded with biotinylated ladder, chemiluminiscent substrate, primary antibodies (rabbit polyclonal anti-RBM20[15] and anti-αTubulin DM1A (Calbiochem)) and secondary antibodies onto the designated wells in a pre-microplate (ProteinSimple) prefilled with separation gel. Automated electrophoresis (375 V, 25 min, Antibody diluent time 5 min, primary & secondary antibody time 30 min) and immunodetection were performed following manufacturer's instructions. For data analysis, we used the Compass Software (ProteinSimple). The area under the curve of the protein of interest was divided by (normalized) the area under the curve of the loading control protein (α-Tubulin) peak. Representative ("virtual blot") electrophoretic images were automatically generated by the Compass Software (ProteinSimple).

RNA sequencing

Two RNA sequencing experiments were performed. The first RNA-seq experiment was done to identify the splicing effect of the RBM20 mutations on two-month-old iPSC-CMs of five genotypes (P663L, R634Q, S635FS, WT, and WT-NC) each with three replicates from independent differentiations. A second experiment was performed to test and validate the effect of ATRA on two-month-old WT, DCM1, and S635FS iPSC-CM of four replicates from three independent differentiations. RNA was purified using TRizol extraction and isopropanol precipitation. For the first experiment total RNA (2-10 ng) was reverse transcribed to generate full-length complementary DNA (cDNA) using SmartSeq2 (Picelli et al., 2014). Then, 100-200 pg of full-length cDNA was tagmented using Illumina's Nextera XT kit to generate fragments with a median length of 500 bp for the addition of the sequencing index adapters as described by the manufacturer's protocol. Multiple samples with different sequencing indexes were pooled and sequenced on multiple Illumina HiSeq lanes at an average depth of 100 million reads per sample. For the second experiment, after DNAase and depletion of ribosomal RNA treatment, libraries were prepared using the Trueseq protocol. Multiple samples with different sequencing indexes were pooled and sequenced on multiple Illumina Nextseq runs with 75 pair end reads at an average depth of 60 million reads per sample for the second experiment. RNA-Seq reads were mapped to GRCh38 using STAR v2.5.1b. Gene expression levels were determined with featureCounts v1.6.0 (Liao et al., 2014). For each exon, inclusive and exclusive reads were defined. Inclusive reads are reads that include the exon of interest. Exclusive reads are reads that include both the upstream and downstream exon but not the exon of interest. Inclusive and exclusive reads were counted directly from the BAM files using a custom script. Percentage of Spliced-In (PSI) is the ratio of inclusive reads to the sum of inclusive and exclusive reads. We identified differentially expressed genes using DESeq2 v1.22.0 with the effect from genotype or differentiation regressed out (e.g., Expression ~Condition + Genotype in the first experiment, or Expression ~Treatment + Differentiation in the second experiment). Adjusted p values were calculated using Benjamini & Hochberg method. We detected alternative splicing with DEXSeq v1.16.10 (Anders et al., 2012). The mean of the counts across all samples for each exon was extracted from DEXSeq. Exons with an average of less than 64 (2^6) counts were excluded. We considered an exon as alternatively spliced when DEXSeq padj (adjusted p value, Benjamini & Hochberg) was < 0.05 and the difference in the median of PSI values was > 0.1. We identified 20 significant differentially spliced genes with one exon each. Two exceptions were *TTN* and *CAMK2D*. For *TTN* we only reported the most significant exon because several exons were affected, all being preferentially included in the *RBM20* mutant lines. For *CAMK2D* two mutually exclusive exons were affected: one is preferentially included in the WT iPSC-CMs (*CAMK2D-E14* in Figures 2A and S2B) and one is preferentially included in the *RBM20* mutant iPSC-CMs (*CAMK2D-E15* in Figures 2A and S2B).

qRT-PCR

To analyze transcript expression in C2C12 cells total RNA was extracted from cultured cells using ReliaPrep RNA Tissue Miniprep System (Promega, Madison WI, USA) according to the manufacturer's instructions. 2 μg of total RNA were reverse transcribed using the High-Capacity RNA-to-cDNA Kit (Life Technologies GmbH, Darmstadt, Germany). Quantitative RT-PCR was performed using SYBRGreen master mix (Applied Biosystems by Thermo Fisher Scientific Inc., USA) on a 7900 HT RT-cycler (Applied Biosystems by Thermo Fisher Scientific, Inc., USA). To quantify gene expression, we used the $\Delta\Delta C_T$ method. PSI values were calculated as a ratio of unspliced to spliced reporter transcript. Primer sets are previously published (Liss et al., 2018). N = 3 samples were used. Comparison between groups used Dunnett's post-test against CTRL.

To analyze transcript isoforms in iPSC-CMs, two-month-old cardiomyocytes from 3 independent differentiation experiments were collected, RNA was purified using TRizol extraction and isopropanol precipitation, and reverse transcription was performed on 500 ng of total RNA using SuperScript® VILO cDNA Synthesis Kit (Life Technologies), following manufacturer's instructions. PCR was performed using PrimeSTAR GXL DNA Polymerase from Takara Bio. Quantitative RT-PCR (qRT-PCR) was performed with Bio-rad SYBR® Green Master Mix. Primer sequences are provided in Table S4. Relative transcript expression to control was calculated using the ΔΔCt method as previously described (Livak and Schmittgen, 2001). For ATRA treatment 2-3 wells from each differentiation

were used for each condition for a final n = 6-8. Wilcox test was used to calculate p values. Before comparing across batches, mean centering batch correction was applied. Adjusted p values were calculated with the FDR method.

Image acquisition

For imaging experiments, cells were dissociated and plated onto Matrigel-coated 384-well tissue culture plates (Greiner Bio-One) at a density of $2x10^4$ cells/well. Cells were allowed to recover for 4 days changing media every second day. All cell manipulations were conducted in a cell culture cabinet on a 37°C dry heat block and all the solutions were pre-warmed to 37°C to prevent temperature fluctuations. Cells were washed 4 times with Fluorobrite (Thermo Fisher A1896701). For contractility analysis, cells were loaded for 15 min with 4 μg/ml of Hoechst 33258 (H3569, Life Technologies) and 10 μg/ml of wheat germ agglutinin–Alexa Fluor 488 conjugate (W11261, Life Technologies) in Fluorobrite. Time series images were acquired automatically using the IC200 KIC instrument (Vala Sciences, California, USA) at an acquisition frequency of 100 Hz for a duration of 10 s, with excitation wavelength of 485/20 nm and emission filter 525/30 nm using a 0.75 NA 20x Nikon Apo VC objective. A single image of the Hoechst stain was acquired after the time series. For each condition and cell line 6 wells from each of 2 independent differentiations were analyzed (n = 12).

For calcium analysis, cells were loaded for 20 min with 4 μg/ml of Hoechst 33258 and 2.7 μM Fluo-4NW (Thermo Fisher F36206) in Fluorobrite. After fluorophore loading, cells were washed 4 more times before image acquisition. Time series images were acquired automatically using the IC200 KIC instrument (Vala Sciences, California, USA) at an acquisition frequency of 100 Hz for a duration of 10 s, with excitation wavelength of 485/20 nm and emission filter 525/30 nm using a 0.75 NA 20x Nikon Apo VC objective. A single image of the Hoechst stain was acquired after the time series. For each condition and each cell line, 6 wells from each of 3 independent differentiations were analyzed (n = 18).

Image analysis and calculation of physiological parameters

Image analysis and physiological parameter calculation was conducted using commercially available Cyteseer (Vala Sciences) (Cerignoli et al., 2012). Contractility analysis was performed using a custom particle image velocity algorithm. Contractility is quantified as the relative change in area of the beating cells, given by the divergence of the measured deformation field, and reported as the peak divergence amplitude (Serrano et al., 2018; Sharma et al., 2017). Data tables were analyzed using R. Comparisons between multiple groups were evaluated for significance using a two-way ANOVA, followed by multiple comparison of means using Tukey's test.

QUANTIFICATION AND STATISTICAL ANALYSIS

Error bars represent standard deviations unless otherwise specified. For pairwise comparison we used the Student's t test or the Wilcox test as appropriate. To compare multiple groups, we used two-way ANOVA to account for batch effect, followed by multiple comparison of means using Tukey's test. Further details are provided in the context of each specific assay in the relevant section of the Method Details.